

Supporting Information

Elucidating the effects of composition on hydrogen sorption in TiVZrNbHf-based High Entropy Alloys

Gustav Ek^{1*}, Magnus M. Nygård², Adriano F. Pavan¹, Jorge Montero³, Paul F. Henry^{1,4}, Magnus H. Sørby², Matthew Witman⁵, Vitalie Stavila⁵, Claudia Zlotea³, Bjørn C. Hauback², Martin Sahlberg¹

¹Department of Chemistry – Ångström laboratory, Uppsala University, Box 523, SE-75120, Uppsala, Sweden

²Institute for Energy Technology, Department for Neutron Materials Characterization, P.O. Box 40, Kjeller NO-2027 Norway

³Université de Paris Est, Institut de Chimie et des Matériaux Paris Est, CNRS, UPEC, 94320 Thiais, France

⁴ISIS Pulsed Neutron and Muon source, Rutherford Appleton Laboratory, OX11 0QX, Didcot, United Kingdom

⁵Sandia National Laboratories, Livermore, California 94551, United States

*Corresponding author: gustav.ek@kemi.uu.se

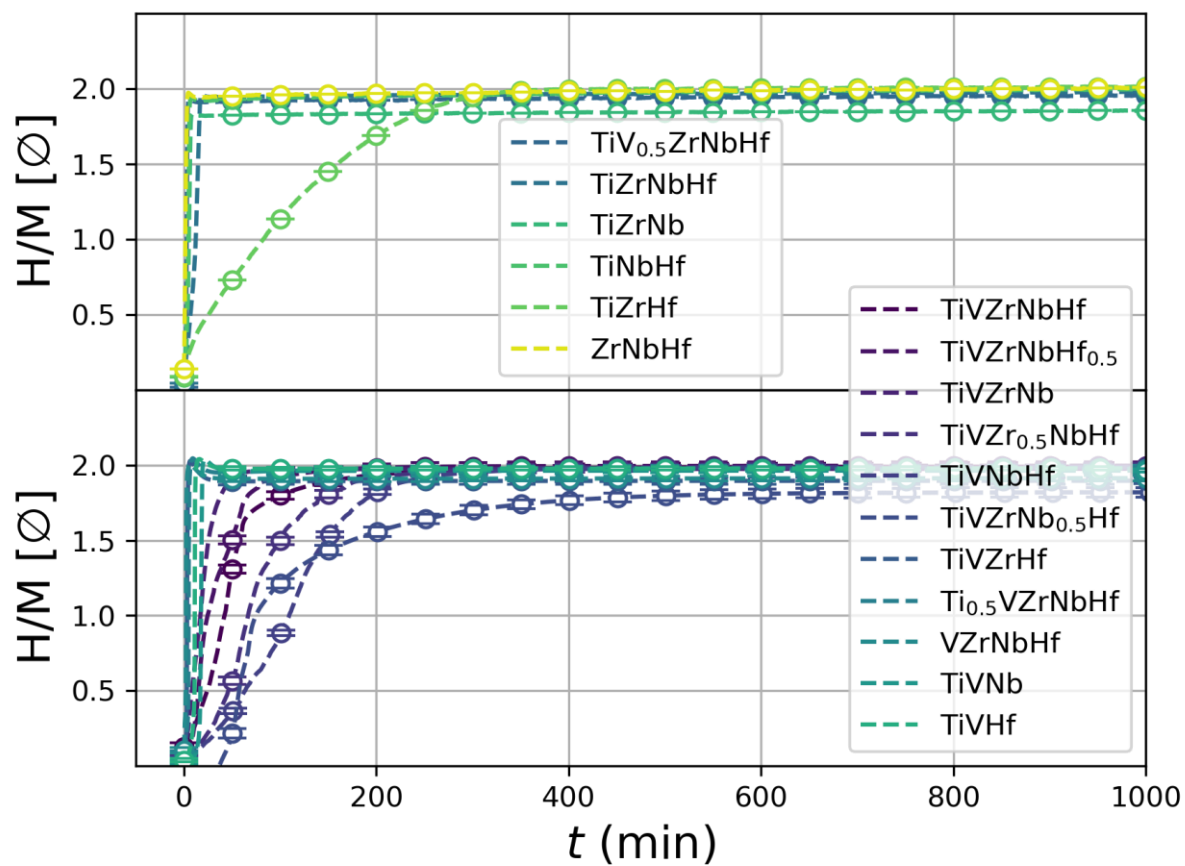


Figure S1: Hydrogen absorption kinetics after exposure to 40 bar H_2 at RT (bottom) and 300°C (top).

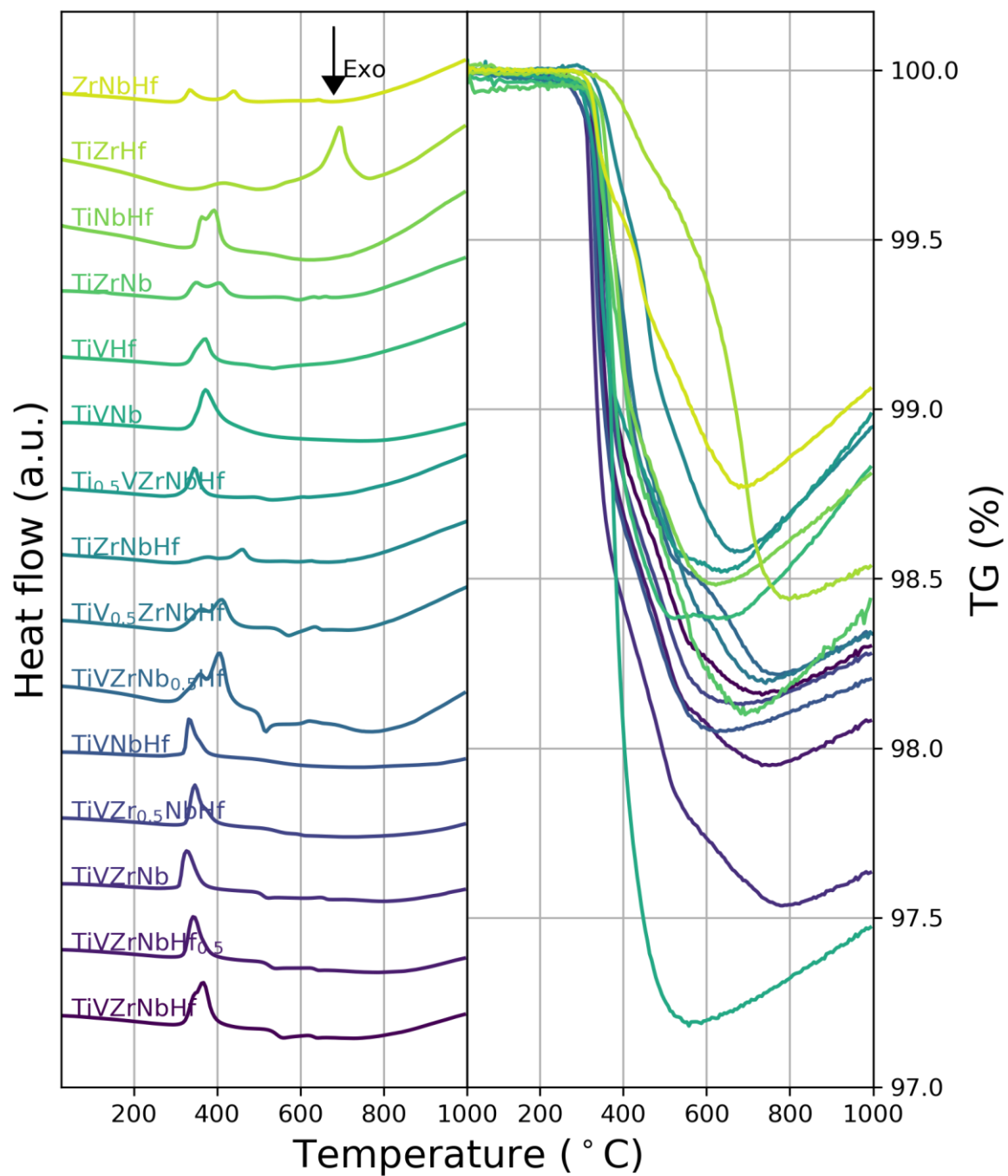


Figure S2: TG (right) and DSC (left) traces during hydrogen desorption at 10 °C/min.

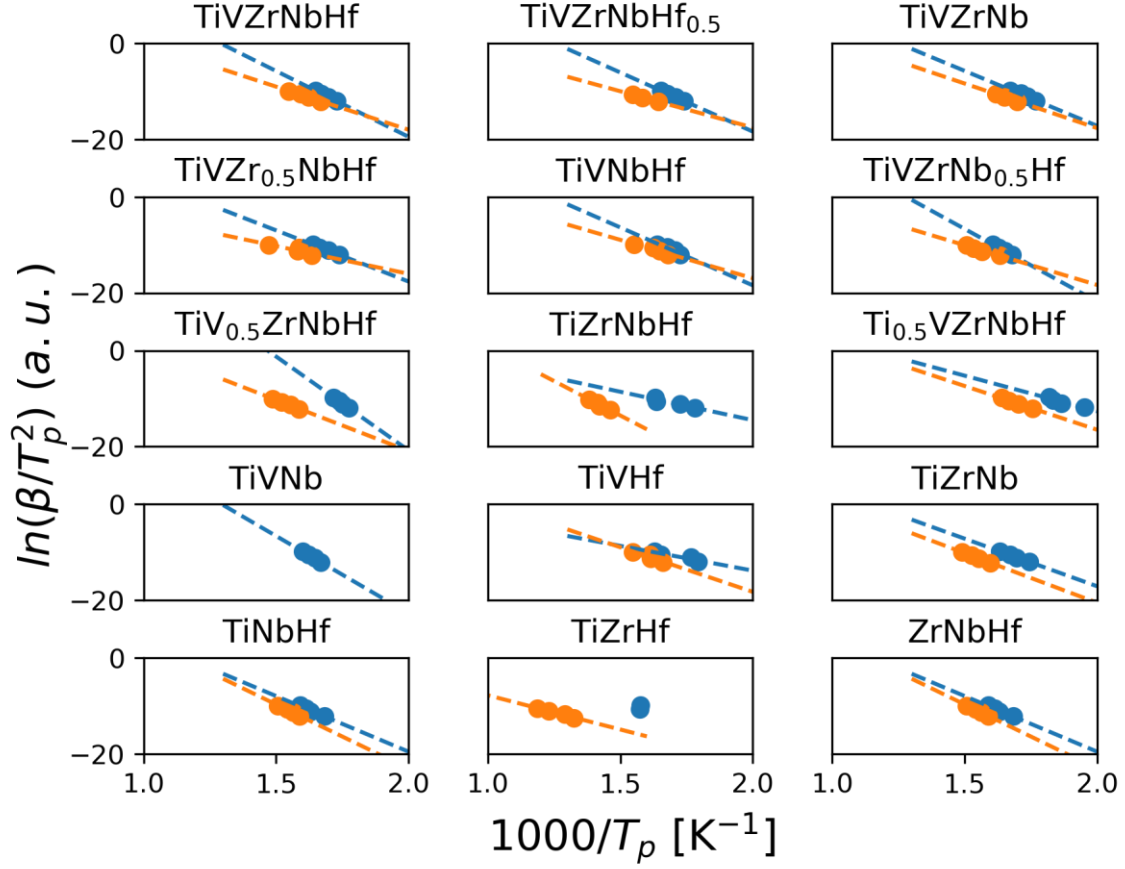


Figure S3: Kissinger analysis for the hydrogen desorption for the first (blue) and second (orange) desorption events.

Table S1: Calculated coherent neutron scattering cross sections for selected compositions using neutrons with wavelength 1.5 Å.

Composition	Neutron scattering cross section (1/cm)
TiVNbD ₆	0.402
TiVNb	0.009
TiVZrNbD ₈	0.458
TiVZrNb	0.047
TiVZrNbHfD ₁₀	0.505
TiVZrNbHf	0.087

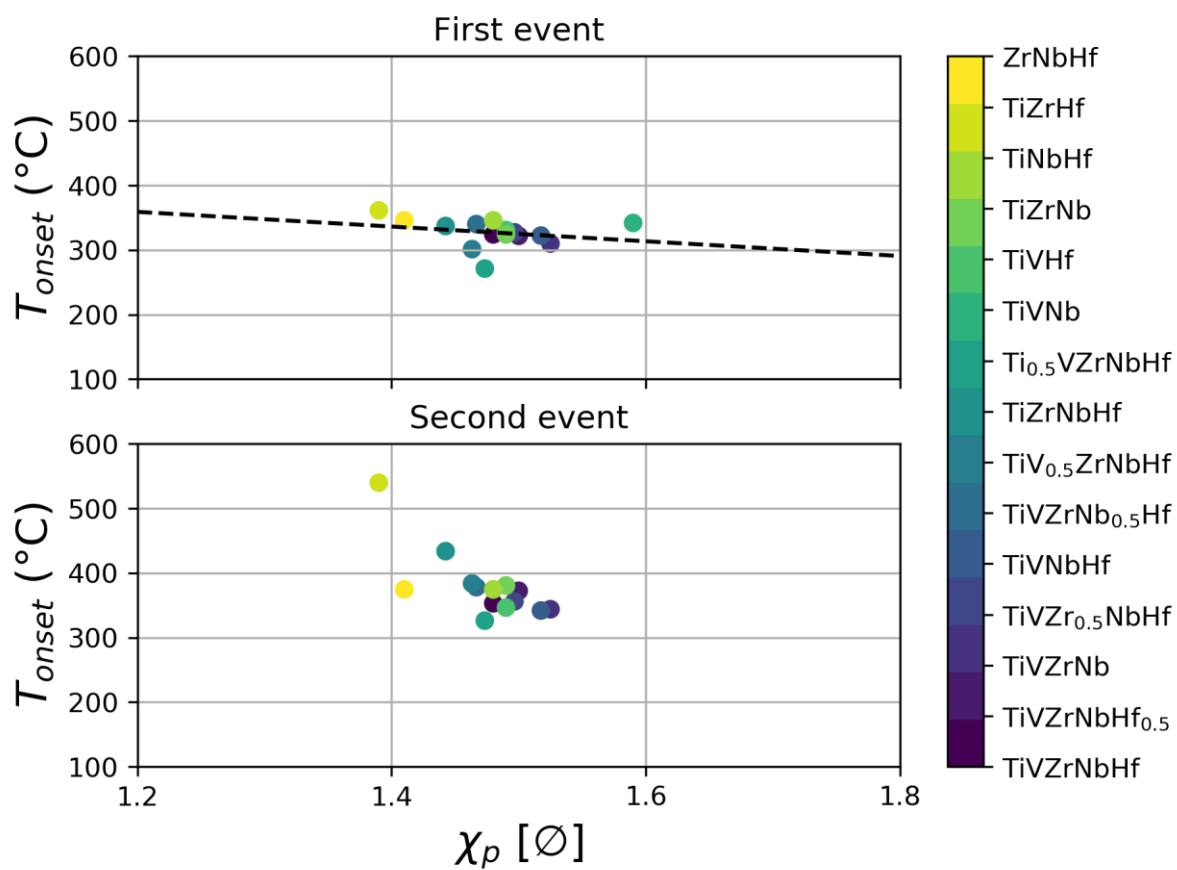


Figure S4: The onset temperature of the first (top) and second (bottom) desorption events as a function of the mean Pauling electronegativity.

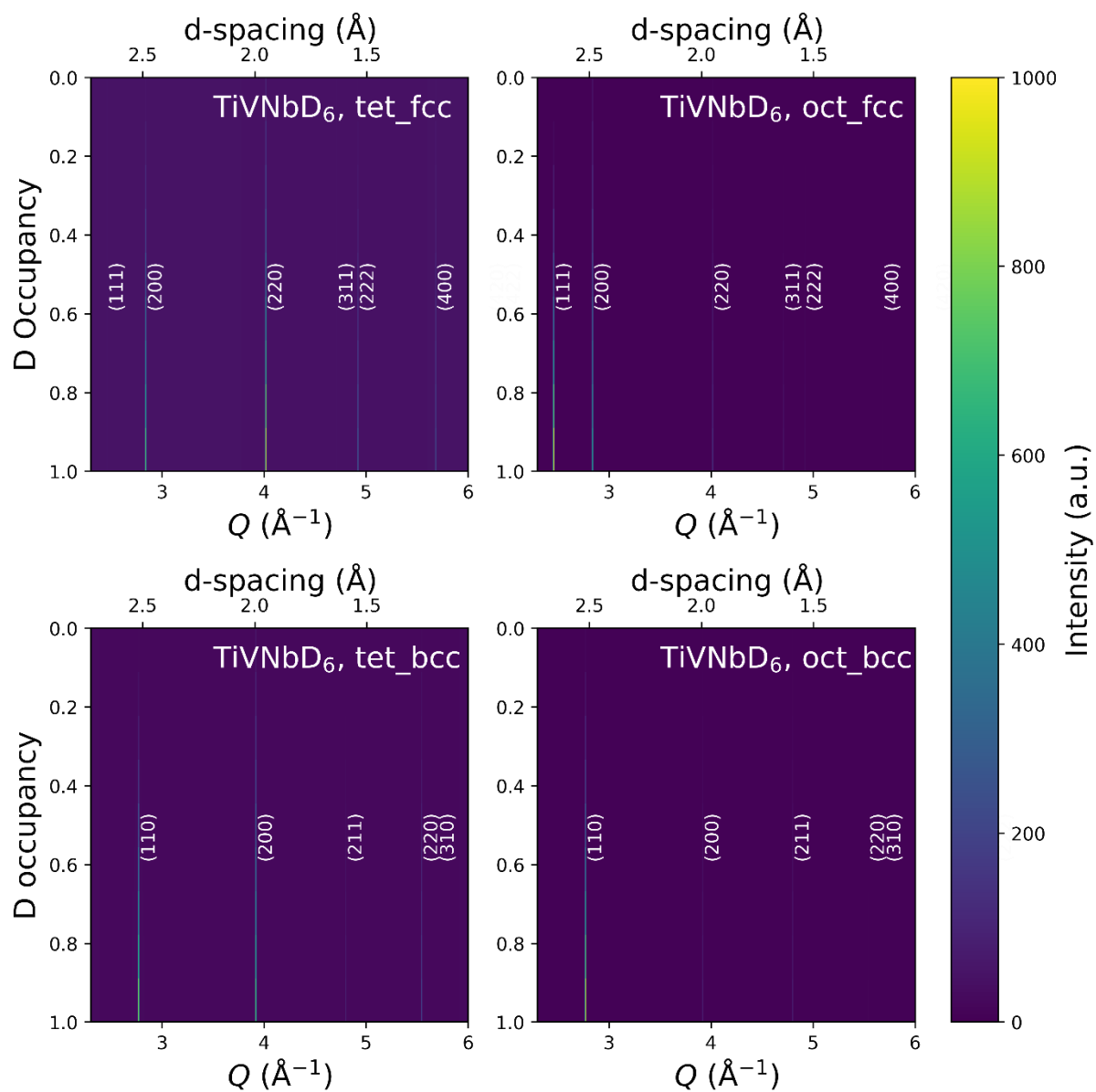


Figure S5: Simulated neutron powder diffraction patterns for TiVNbD_6 with different deuterium occupancy factors and constant unit cell parameter.

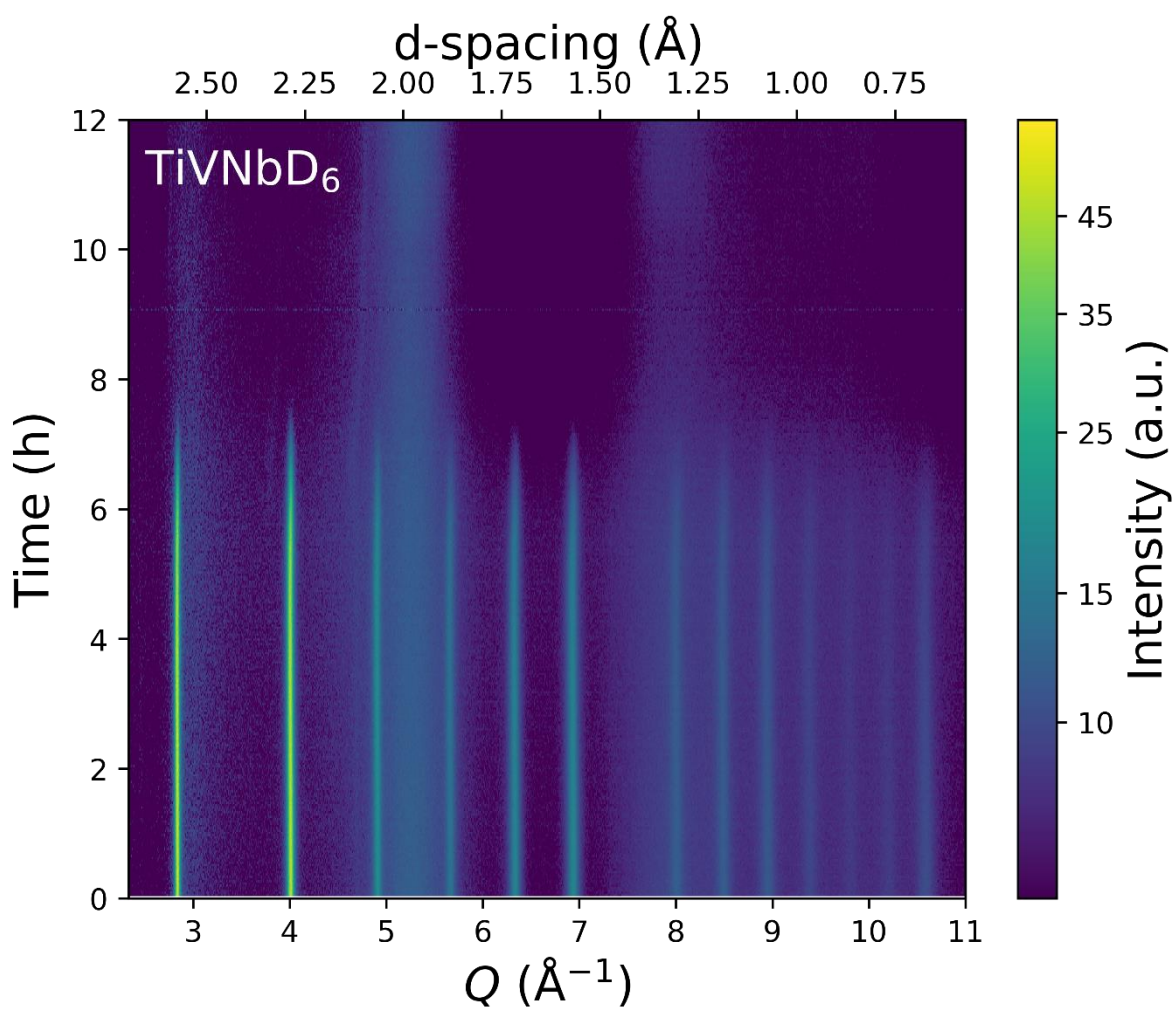


Figure S6: In-situ neutron powder diffraction from the backscattering bank of Polaris during desorption of TiVNbD_6 .

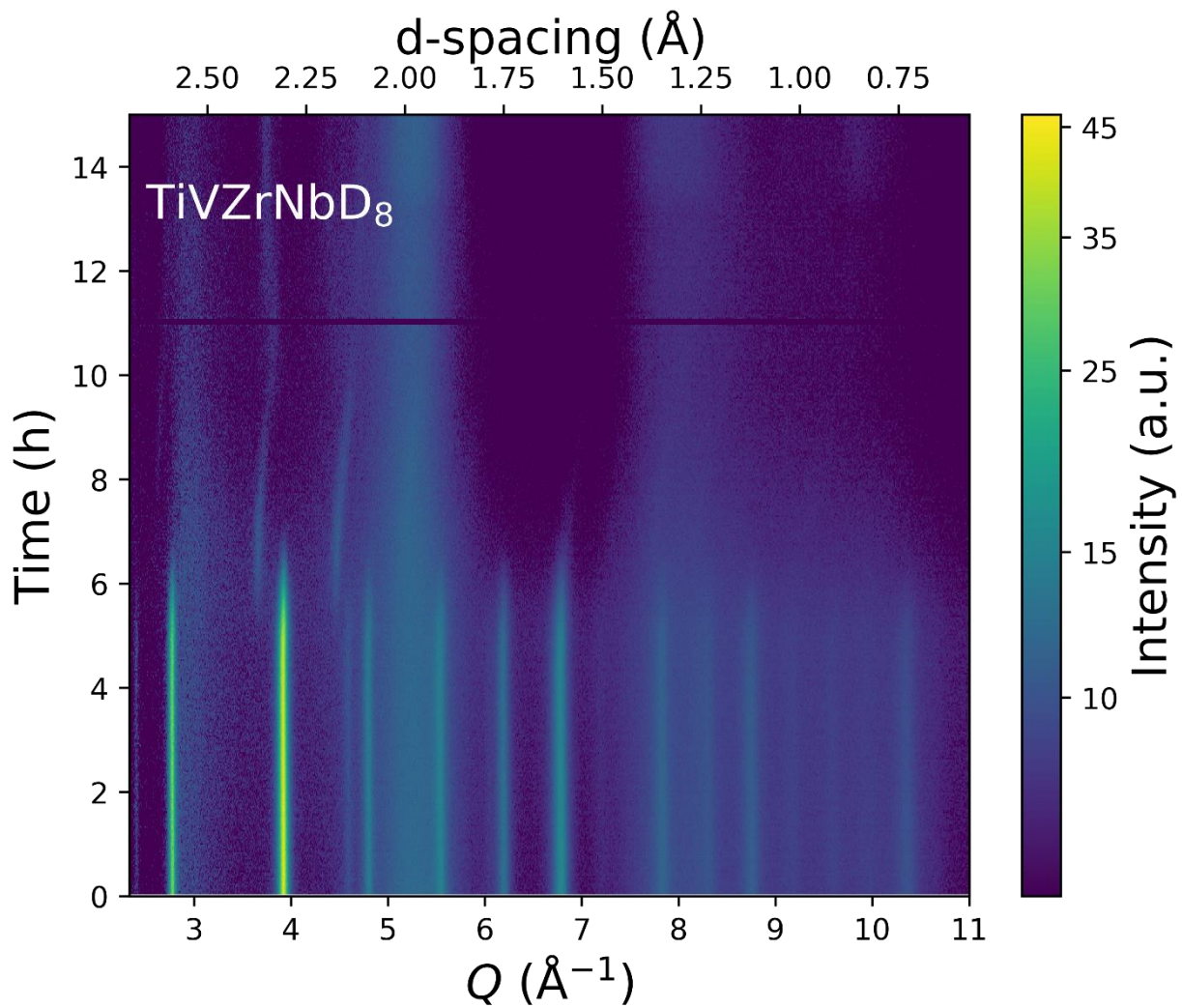


Figure S7: In-situ neutron powder diffraction from the backscattering bank of Polaris during desorption of TiVZrNbD_8 .

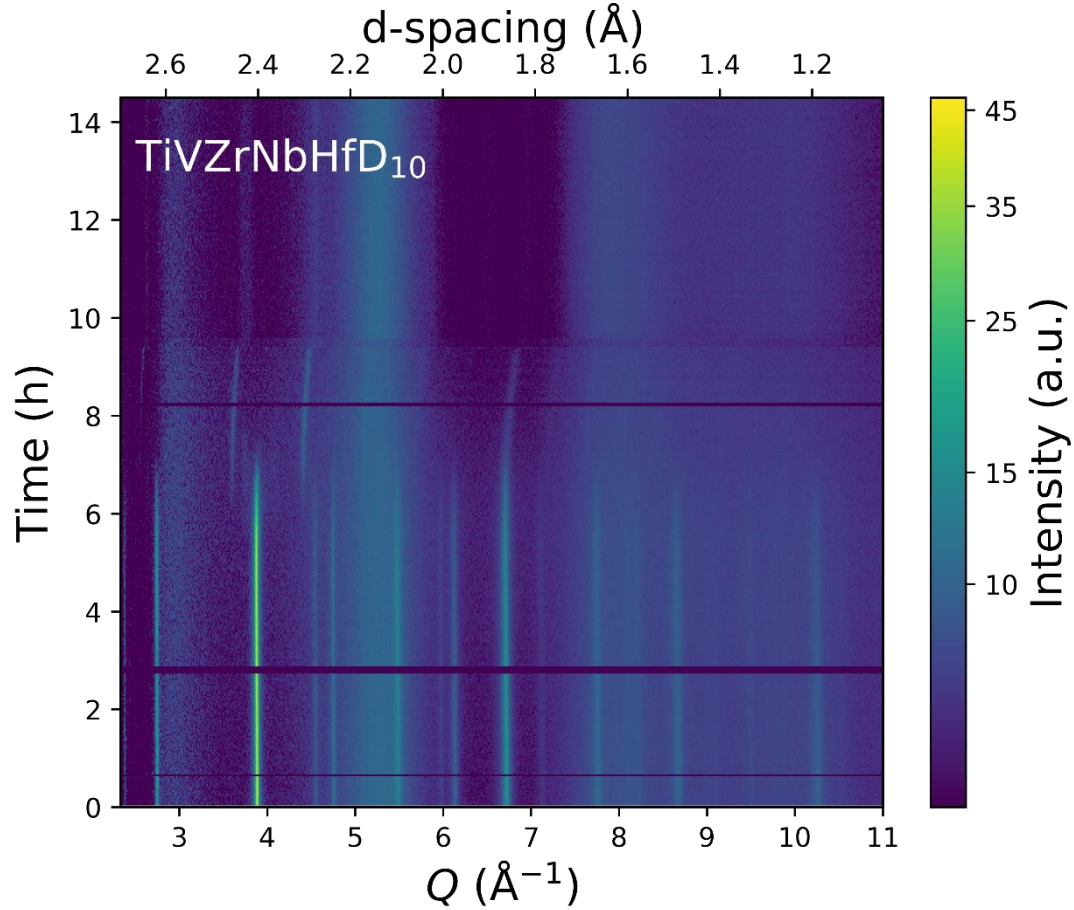


Figure S8: In-situ neutron powder diffraction from the backscattering bank of Polaris during desorption of TiVZrNbHfD_{10} .

Table S2: Crystallographic information and refinement strategies for the in-situ neutron diffraction data.

	Site	Wyckoff	x	y	z	occupancy	flag	limits
<i>Fm-3m</i>								
	Metal	4a	0	0	0	nominal	fixed	none
	D_tet	8c	0.25	0.25	0.25	$0 < x < 1$	refined	Total occupancy constrained by TG information
	D_oct	4b	0.5	0	0	$0 < x < 1$	refined	
<i>Im-3m</i>								
	Metal	2a	0	0	0	nominal	fixed	none
	D_tet	6b	0	0.5	0.5	$0 < x < 1/3$	refined	Total occupancy constrained by TG information
	D_oct	12d	0	0.5	0.25	$0 < x < 1/6$	refined	

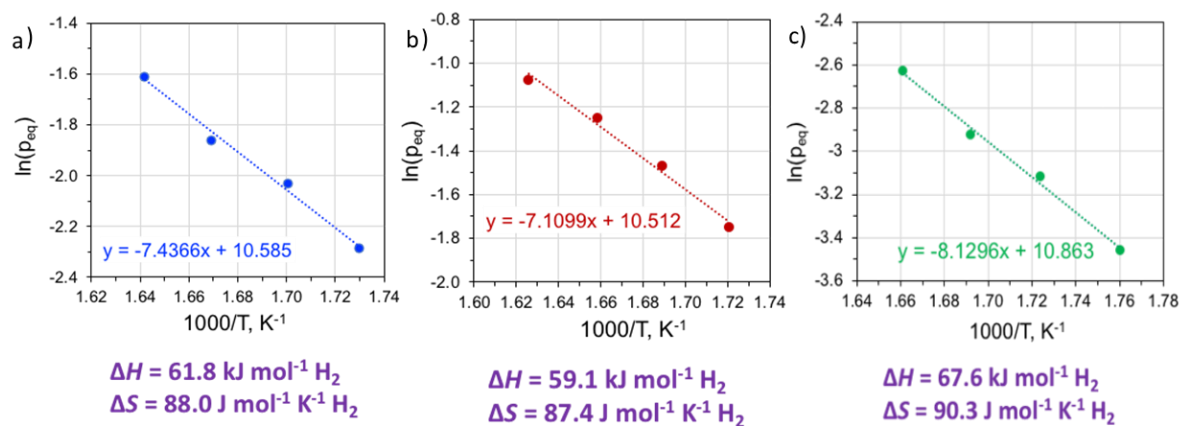


Figure S9: Van 't Hoff plot for a) TiVZrNbHf, b) TiV_{0.5}ZrNbHf and c) TiVZrNb